

STOCHASTIC ANALYSIS OF AN ELECTROMECHANICAL COUPLED SYSTEM WITH EMBARKED MASS

Roberta de Queiroz Lima and Rubens Sampaio

*PUC–Rio, Marquês de São Vicente 225, Gávea, Rio de Janeiro, RJ, Brasil,
roberta_10_lima@hotmail.com, rsampaio@puc-rio.br*

Keywords: Nonlinear dynamics, vibro systems, coupled systems, energy pumping, stochastic analysis.

Abstract. The objective of this paper is to analyze the behavior of embarked vibro systems considering the existence of epistemic uncertainties in the systems parameters. Two different systems were studied. The first one is composed by a cart whose motion is excited by a DC motor and the second, a pendulum is added into this cart and can have a relative motion with respect to the cart. The electrical motor is modeled as a limited source of power and, its influence in the dynamic behavior of the two systems are considered. The coupling between the motor and the cart is made by a mechanism called *scotch yoke*, so that the motor rotational motion is transformed in horizontal cart motion. The influence of the pendulum embarked in the cart was investigated and it is presented an analysis of the coupling force. In the stochastic analysis, an uncertain parameter is modeled as random variable and, the Maximum Entropy Principle is used to construct its probability model. Monte Carlo simulations are employed to compute the mean and the 90% confidence interval of the displacements of the pendulum, of the cart and of the angular speed of the motor shaft.

1 INTRODUCTION

The wide occurrence of the electromechanical coupling in manufacturing processes turns the research on this topic an area of interest for engineering practice. By coupling it is meant a mutual influence between the systems. In the two systems studied in this paper the source of energy is the imposed voltage that will be taken as constant. The dynamics of the motor is heavily influenced by the coupled mechanical system. To better see the effects of coupling the mechanical system has no dissipation, the only dissipation is in the electrical part. It is believed that the theoretical knowledge on couplings between electric motors and mechanical systems can provide improvements in the design of mechanical systems and can help in the development of control techniques.

Electromechanical coupled systems is not a new subject, in [Rocard \(1943\)](#) there is a chapter dedicated to the coupled problem and it is remarked that it is a problem different from parametric resonance. In [Kononenko \(1969\)](#) the whole book is dedicated to the problem but the analytical treatment supposes some small parameter, a hypothesis avoided here. Recently, the problem is been intensely studied again, see [Belato \(2002\)](#); [Aguilar \(2010\)](#); [Balthazar et al. \(2003\)](#), but the literature is vast. It is important to remark that the nonlinearity of this problem is not prescribed by a function, as is unfortunately found in several papers, but it comes from the coupling and the nonlinearity varies with the coupling conditions. This means that the nonlinearity varies with the dynamics, one cannot that it a sine, or a cubic nonlinearity, as seen in some papers, for example. Coupled problems have a very rich system dynamics due to presence of nonlinearities arising from the mutual interaction of the coupled systems, see [Nayfeh and Mook \(1979\)](#); [Evan-Iwanowski \(1976\)](#); [Fidlin \(2006\)](#); [Hagedorn \(1988\)](#); [Troger \(1991\)](#).

In this paper, it is analyzed and compared two electromechanical systems. The first one is a very simple system composed by a cart whose motion is driven by a DC motor. The coupling between the motor and the cart is made by a mechanism called *scotch yoke*. In this simple system the coupling is a sort of master-slave condition: the motor drives, the cart is driven, and that is all. The second system has the same two elements of the first and also a pendulum that can move relative to the cart. The pendulum introduces a new feature since the motion of the pendulum acts as a reservoir of energy, i.e. energy from the electrical system is pumped to the pendulum and stored in the pendulum motion, changing the characteristics of the mechanical system. The pendulum is the embarked system and its motion is driven by the motion of the cart or, better said, by the motor. The motor is influenced by the attached mass and the heavier the mass the greater the nonlinearities involved. Normally, problems of this type are modeled saying that the forcing is harmonic with frequency given by the nominal frequency of the motor. It will be shown here that this hypothesis is far from true.

Without simplifying hypothesis about the terms, the behavior of the system variables are analyzed, as the motor current over time, rotational movement of the motor shaft and force and torque exerted by the DC motor in the mass. The influence of the pendulum embarked in the cart is investigated and it is shown the changes it causes in the dynamics of the second system with respect to the first.

The two most important parameters of the coupled problem are the attached mass and the amplitude of its motion that is given by the position of the pin used in the coupling. With some simplifying hypothesis a lot of analytical results could have been derived as well as results about chaotic behavior, but this is not the object of the paper. The object is to show the dynamics without undue simplifications.

This paper is organized as follows. Section 2 describes the two coupled electromechanical

systems analyzed. Section 3 presents the results of the deterministic simulations developed to each one of them. The influence of the attached mass and the amplitude of its motion are discussed. In Section 4, it is presented a configuration of the coupled system that leads to the phenomenon of energy pumping and causes revolution, i. e. the inversion of the master-slave relation. The probability model to the parameter that is considered uncertain is construct in Section 5 and the results of the simulations of the stochastic systems are presented in Section 6. Section 7 presents some conclusions.

2 DYNAMICS OF THE COUPLED SYSTEMS

Next, it is presented the elements of the two coupled systems (motor, cart, and pendulum). The coupling between the motor and the mechanical systems are shown and the two coupled problems are described and mathematically formulated as initial-value problems.

2.1 Electrical system: motor DC

The mathematical modeling of DC motors is based on the Kirchhoff's law (Karnopp et al., 2006). It is constituted by the equations

$$l\dot{c}(t) + r c(t) + k_e \dot{\alpha}(t) = v, \tag{1}$$

$$j_m \ddot{\alpha}(t) + b_m \dot{\alpha}(t) - k_t c(t) = -\tau(t), \tag{2}$$

where t is the time, v is the source voltage, c is the electric current, $\dot{\alpha}$ is the angular speed of the motor, l is the electric inductance, j_m is the motor moment of inertia, b_m is the damping ratio in the transmission of the torque generated by the motor to drive the coupled mechanical system, k_t is the torque constant, k_e is the motor electromagnetic force constant and r is the electrical resistance. Figure 1 shows a sketch of a DC motor. The available torque to the coupled mechanical system is represented by τ , that is the component of the torque vector $\vec{\tau}$ in the z direction shown in Fig. 1.

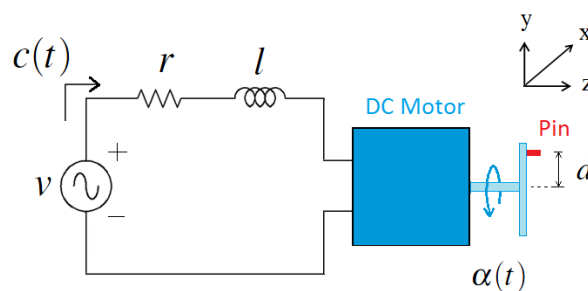


Figure 1: Electrical motor DC.

Assuming that the load applied in the motor and source voltage are constant in time, the motor achieves a steady state. Thus, the electric current and the angular speed become constant and $\ddot{\alpha}(t) = 0 = \dot{c}(t) = 0, \forall t \in \mathbb{R}^{\geq 0}$. By equations (1) and (2), the angular speed of the motor shaft and the current in steady state, respectively $\dot{\alpha}_{steady}$ and c_{steady} , can be calculated by

$$\dot{\alpha}_{steady} = \frac{-\tau r + k_t v}{b_m r + k_e k_t}, \quad c_{steady} = \frac{v}{r} - \frac{k_e}{r} \left(\frac{-\tau r + k_t v}{b_m r + k_e k_t} \right). \tag{3}$$

When the hypothesis of constant load is not verified, the angular speed of the motor shaft and the current do not reach a constant value. This kind of situation happens when, for example, a mechanical system is coupled to the motor. In this case, $\dot{\alpha}$ and c variate in time in a way that the dynamics of the motor will be influenced by the coupled mechanical system.

Two more situations are relevant when we analyze electrical motors. The first one is when there is no load applied in the motor (i.e. $\tau(t) = 0, \forall t \in \mathbb{R}^{\geq 0}$) and the source voltage is constant in time. Then, the motor achieves its maximum angular speed that is called the *no load speed*. It is calculated by

$$\dot{\alpha}_{no\ load} = \frac{k_t v}{b_m r + k_e k_t} . \quad (4)$$

The second one is when the motor delivers the maximum torque. This torque is achieved when the load applied in the motor is such that the motor does not move at all. This is called the *stall torque*. If the source voltage is constant in time, it is calculated by

$$\tau_{stall} = \frac{k_t v}{r} . \quad (5)$$

In the problems discussed here, there is the constraint $\tau(t) < \tau_{stall}$. In Sec. 3 it is taken care do not reach this condition.

2.2 Coupled cart-motor system: a master-slave relation

As described in the introduction, the system analyzed in this paper is composed by a cart whose motion is driven by the DC motor sketched in Fig. 1. The motor is coupled to the cart through a pin that slides into a slot machined on an acrylic plate that is part to the cart, as shown in Fig. 2. The pin hole is drilled off-center on a disk fixed in the axis of the motor, so that the motor rotational motion is transformed into horizontal cart motion.

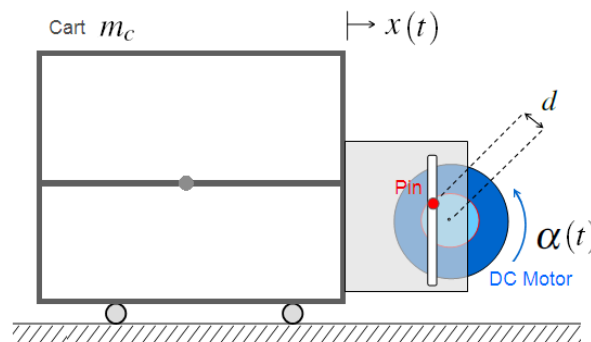


Figure 2: First Mechanical System.

It is noticed that with this configuration, the center of mass of the mechanical system is always located in the center of mass of the cart, so its position does not change.

The mass of the mechanical system, m , is equal the cart mass, m_c , and the horizontal cart displacement is represented by x . Due to constraints, the cart is not allowed to move in the vertical direction. Due to the problem geometry, and noting $\|\vec{d}\| = d$, the horizontal motion of the cart and the angular displacement α of the motor are related by the constraint

$$x(t) = d \cos \alpha(t) . \quad (6)$$

To model the coupling between the motor and the mechanical system, it is assumed that the motor shaft is rigid. Thus, the available torque to the coupled mechanical system, $\vec{\tau}$, can be written as

$$\vec{\tau}(t) = \vec{d}(t) \times \vec{f}(t), \quad (7)$$

where \vec{d} is the eccentricity of the pin of the motor and \vec{f} is the coupling force between the DC motor and the cart. By the problem geometry, the module of \vec{d} is the nominal eccentricity of the pin. Besides this, the component of \vec{d} that is perpendicular to the plane of the cart movement is always zero and, the others horizontal and vertical components can be calculated from the angular displacement α of the motor.

Assuming that there is no friction between the pin and the slot machined on an acrylic plate, the vector \vec{f} only has a horizontal component, f (the horizontal force that the DC motor exerts in the cart). Thus, \vec{d} and \vec{f} are written as

$$\vec{d}(t) = \begin{bmatrix} d \cos \alpha(t) \\ d \sin \alpha(t) \\ 0 \end{bmatrix} \quad \vec{f}(t) = \begin{bmatrix} f(t) \\ 0 \\ 0 \end{bmatrix}. \quad (8)$$

Substituting Eq. (8) in Eq. (7), the module of $\vec{\tau}(t)$ is

$$\tau(t) = -f(t)d \sin \alpha(t). \quad (9)$$

Since the cart is modeled as a particle, it satisfies the equation

$$m \ddot{x} = f(t). \quad (10)$$

Substituting the Eq. (9), (6) and (10) in the equations of the electric motor, we obtain a system of differential equations to the coupled system.

The initial value problem for the motor-cart system is: given the source voltage of the motor, v , find (α, c) satisfying

$$\begin{aligned} l\dot{c}(t) + r c(t) + k_e \dot{\alpha}(t) &= v, \\ \ddot{\alpha}(t) \left[j_m + m d^2 (\sin \alpha(t))^2 \right] + \dot{\alpha} \left[b_m + m d^2 \dot{\alpha}(t) \cos \alpha(t) \sin \alpha(t) \right] - k_t c(t) &= 0, \end{aligned} \quad (11)$$

for given initial conditions.

Comparing Eqs. 1, 2, and 11 it is seen that the attached mass influences the motor in a parametric way, [Lacarbonara and Antman \(2008\)](#).

2.3 Coupled cart-motor-pendulum system: introduction of a mechanical energy reservoir

In the second system, a third element, a pendulum, is added to the first system. It is placed inside the cart, as shown in Fig. 3. The suspension point O is fixed in the cart, hence moves with it. The important point is that it can have a relative motion with respect to the cart. That is the meaning we give to *embarked*.

The pendulum with concentrated mass is represented by m_p , the pendulum length by l_p and the pendulum angular displacement by θ .

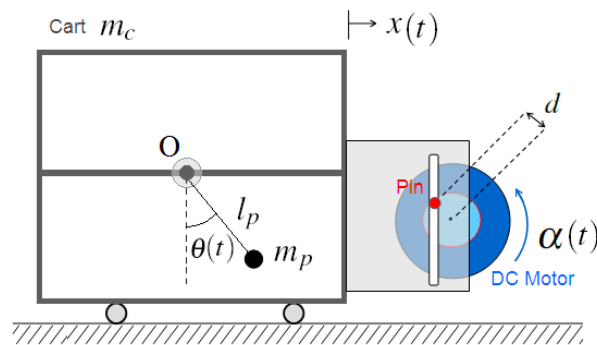


Figure 3: Second Mechanical System.

Using the Lagrangian equation $\mathcal{L} = \mathcal{T} - \mathcal{V}$, with the angle θ and displacement x of the cart as generalized coordinates, the kinetic and potential energies of the mechanical system, are defined respectively as

$$\mathcal{T} = \frac{1}{2}m_p[(l_p\dot{\theta}\cos\theta + \dot{x})^2 + (l_p\dot{\theta}\sin\theta)^2] + \frac{1}{2}m_c\dot{x}^2, \quad (12)$$

$$\mathcal{V} = -m_pg(l_p\cos\theta). \quad (13)$$

Thus, the equation of the cart-pendulum are

$$m_pl_p^2\ddot{\theta}(t) + m_pl_p\ddot{x}(t)\cos\theta(t) + m_pg l_p\sin\theta(t) = 0, \quad (14)$$

$$(m_p + m_c)\ddot{x}(t) + m_pl_p\ddot{\theta}(t)\cos\theta(t) - m_pl_p\dot{\theta}^2(t)\sin\theta(t) = f(t), \quad (15)$$

where, again, f represents the horizontal coupling force between the DC motor and the cart, g is the gravity and the horizontal cart displacement is x .

The relative motion of the embarked pendulum causes a variation in the position of the center of mass of the mechanical system. In this case, the mass of the mechanical system, m , is equal the cart mass plus the pendulum mass, $m_c + m_p$.

As in the first coupled system, the cart is not allowed to move in the vertical direction. Due to the problem geometry, the horizontal motion of the cart and the angular displacement α of the motor are related by Eq. (6).

Once again, it is assumed that the motor shaft is rigid and that there is no friction between the pin and the slot machined on the acrylic plate. Thus, the available torque to the coupled mechanical system, $\vec{\tau}$, is written as Eq. (9).

Substituting the Eq. (9), (6) and (15) in the equations of the electric motor and in Eq. (14), we obtain a system of differential equations for the coupled system.

Given the source voltage of the motor, v , the dynamic of the coupled system is written in terms of the variables α , c and θ . Thus, the initial value problem for the motor-cart-pendulum

system is: given the source voltage of the motor, v , find (α, c, θ) satisfying

$$\begin{aligned}
 l\dot{c}(t) + rc(t) + k_e\dot{\alpha}(t) &= v, \\
 \ddot{\alpha}(t) \left[j_m + (m_c + m_p)d^2(\sin \alpha(t))^2 \right] + \dot{\alpha}(t) \left[b_m + (m_c + m_p)d^2\dot{\alpha}(t) \cos \alpha(t) \sin \alpha(t) \right] + \\
 + k_t c(t) - \ddot{\theta}(t) \left[m_p l_p \cos \theta(t) d \sin \alpha(t) \right] + \dot{\theta}(t) \left[m_p l_p \dot{\theta}(t) \sin \theta(t) d \sin \alpha(t) \right] &= 0, \\
 \ddot{\theta}(t) \left[m_p l_p^2 \right] - \ddot{\alpha}(t) \left[m_p l_p \cos \theta(t) d \sin \alpha(t) \right] - \dot{\alpha}(t) \left[m_p l_p \cos \theta(t) d \cos \alpha(t) \dot{\alpha}(t) \right] + \\
 + m_p g l_p \sin \theta(t) &= 0,
 \end{aligned} \tag{16}$$

for given initial conditions.

3 NUMERICAL SIMULATIONS OF THE DYNAMICS OF THE COUPLED SYSTEMS

To better comprehend the behavior of the coupled systems composed by the DC motor and the mechanical systems, we started analyzing the deterministic models. Simulations of the two systems are compared in order to observe the influence of the pendulum in the rotational motion of the motor shaft.

3.1 Simulations of the motor-cart system

Looking at the initial value problem Eq. (11), it is observed that if the nominal eccentricity of the pin, d , is small, Eq. (11) tends to the linear system equations of the DC motor, Eq. (1) and (2), in case of no load. But as the eccentricity grows, the non-linearities become more pronounced. The nonlinearity also increases with the attached mass, m . To better comprehend the increase of nonlinearity, the system Eq. (11), was integrated in a range of [0.0, 2.0] seconds for different values of d and m .

In the first analysis, d was fixed as 0.005 [m] and the cart mass was varied from 1 [Kg] to 5 [Kg]. In the second analysis, the cart mass was considered to be $m = 5.0$ [Kg] and d was varied in the range 0.001 [m] to 0.01 [m].

The specifications of the motor parameters used in all simulations are listed in Table 1. These values were obtained from the specifications of the motor Maxon DC brushless number 411678. The source voltage was assumed to be constant in time and equal to 2.4 [Volt]. This value is just 10% of the nominal voltage of this motor, 24 [Volt], but it ensures the respect to the constraint $\tau(t) < \tau_{stall}$ for the parameters considered for the coupled system. So the simulations reflect realisable situations.

| Motor Parameter | Notation | Used value | Unit |
|---|----------|------------------------|----------------------|
| Electric inductance | l | 1.880×10^{-4} | [H] |
| Motor moment of inertia | j_m | 1.210×10^{-4} | [Kg m ²] |
| Damping ratio in the transmission of the torque | b_m | 1.545×10^{-4} | [Nm/(rad/s)] |
| Electrical resistance | r | 0.307 | [ohm] |
| Torque constant | k_t | 5.340×10^{-2} | [Nm/Amp] |
| Electromagnetic force constant | k_e | 5.330×10^{-2} | [Volt/(rad/s)] |

Table 1: Motor parameters used in the simulations.

In the integration, the initial conditions assumed for the current in the motor and for the

angular position and velocity of the motor shaft were, in all simulations:

$$\alpha(0) = 0.0 \text{ [rad]}, \quad \dot{\alpha}(0) = 0.0 \text{ [Hz]}, \quad c(0) = v/r = 7.81 \text{ [Amp]}. \quad (17)$$

Due to the coupling mechanism, coupling torque, τ , varies in time. Thus, the angular speed of the motor shaft and the current are not constant values after the transient. As the motor-cart system does not have any mechanism of storing energy, after the transient the dynamics achieves a periodic state. Therefore, to compare the response of the coupled systems for different values of d and m , the duration of one cart movement cycle were computed in the periodic state. Figures 4(a) and 4(b) show the graphs of the computed periods in function of d and m . In both graphs it is observed that, the bigger d or m is, the bigger is the period of the cart movement cycle in the periodic state. It is noted too that this increment is more pronounced in relation to d .

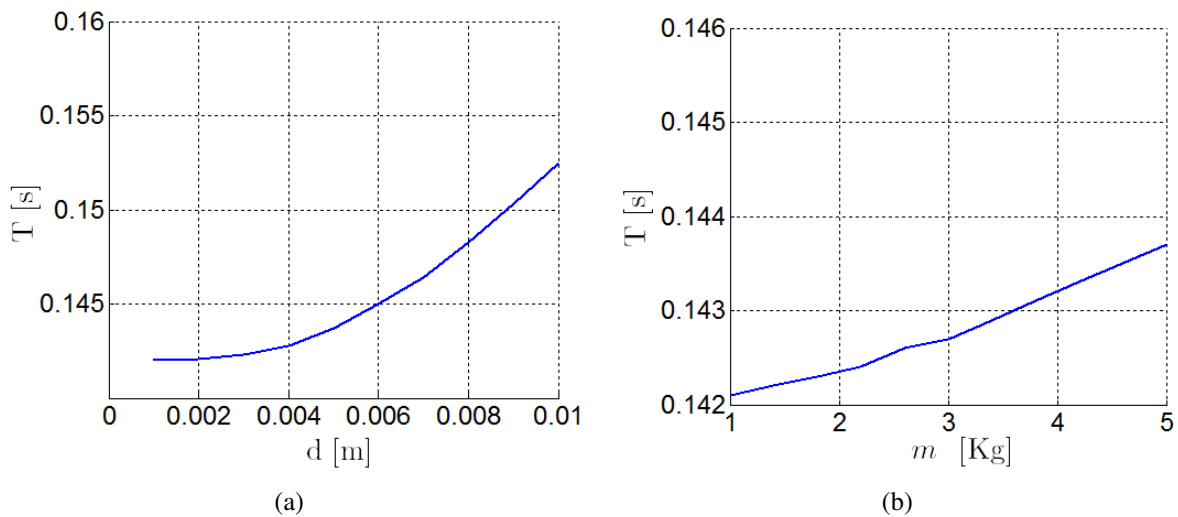


Figure 4: Motor-cart system: (a) period of one cart movement cycle in function of d and (b) in function of m .

Although these graphs show the relation between d or m and the period of the cart, they do not give a more detailed analysis of the motor-cart system. To better comprehend the behavior of the coupled system, is necessary to study the variation of the other variables, as the motor current and the coupling force and torque. To make these analysis, the mass was fixed to 5 [Kg] and two values of d were selected: 0.001 [m] and 0.010 [m]. The selection guarantees that the stall torque is not reached in the simulations.

The Fast Fourier Transform of the cart displacement over time, \hat{x} , was computed for the two different values of d . Figures 5(b) and 6(b) show the obtained results. It is noted that when d is small, as 0.001 [m], the angular speed of the motor shaft oscillates with a small amplitude around 7 [Hz] and the FFT graph of x presents only one peak at this frequency. In contrast to this, when d is bigger, the amplitude of the oscillations of $\dot{\alpha}$ grows and, due to the non-linearity effects, the FFT graph of x presents more than one peak. The first one of them is at 6.56 [Hz] and, the following are at odd multiples of this value.

As said in the introduction of this paper, normally problems of coupled systems are modeled saying that the force is imposed, so no coupling, and it is harmonic with frequency given by the nominal frequency of the motor. The dynamic of the motor is not considered. The graphs of

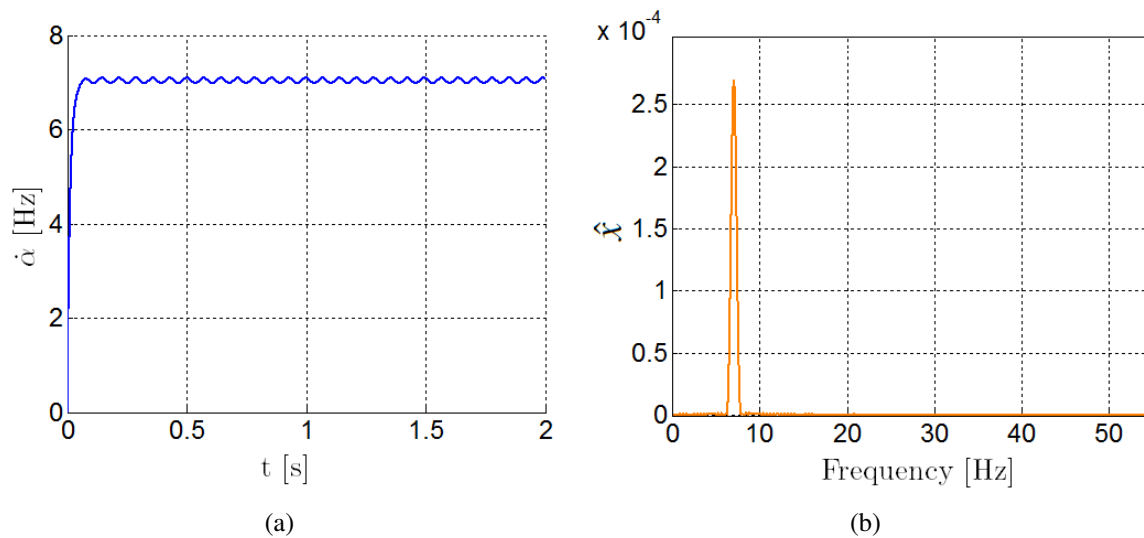


Figure 5: Motor-cart system $d = 0.001$ [m]: (a) angular speed of the motor shaft over time and (b) Fast Fourier Transform of the cart displacement.

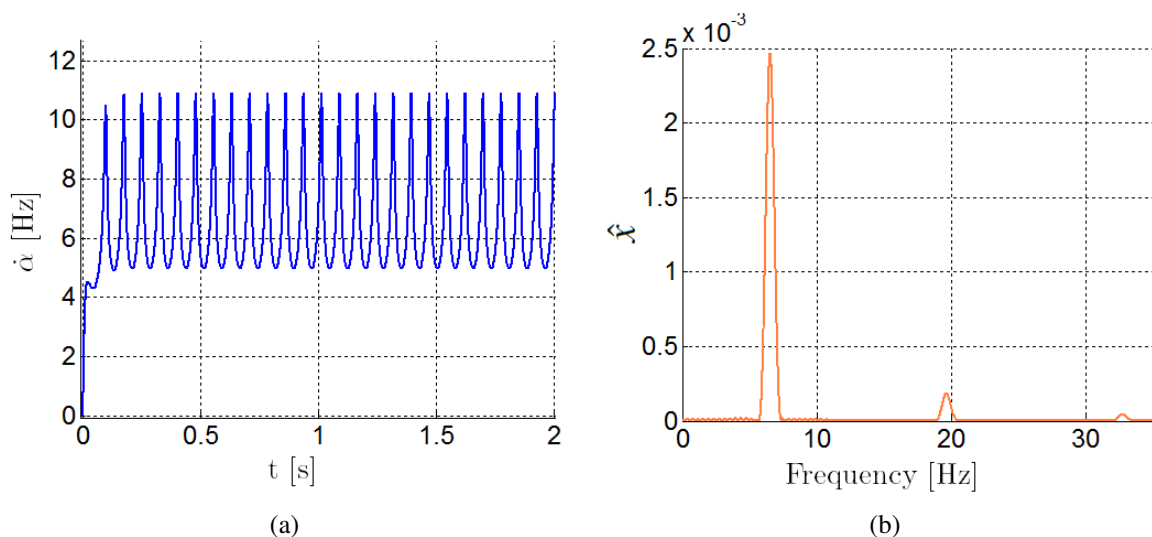


Figure 6: Motor-cart system $d = 0.01$ [m]: (a) angular speed of the motor shaft over time and (b) Fast Fourier Transform of the cart displacement.

Fig. 5(a) and 6(a) confirm that this hypothesis does not correspond to reality. Even when d is small, the angular speed of the motor shaft do not reach a constant value. After a transient it achieves a periodic state. It oscillates around a mean value and these oscillations are periodic.

To enrich the analysis in the frequency domain, the Fast Fourier Transform of the current over time, \hat{c} , was computed for the two values of d . The results are shown in Fig. 7(a) and 7(b). It is observed that in both cases, the FFT graph of \hat{c} presents a peak at a frequency that is twice the peak frequency of the FFT \hat{x} indicating a parametric excitation, [Lacarbonara and Antman \(2008\)](#).

In the following analysis of the motor-cart system, the nominal eccentricity of the pin was considered to be 0.01 [m]. This value was selected to highlight the non-linearity effects. The integration results obtained to the cart displacement and current in motor over time are observed in Fig. 8(a) and Fig. 8(b). The behavior found for the current over time is similar to the behavior

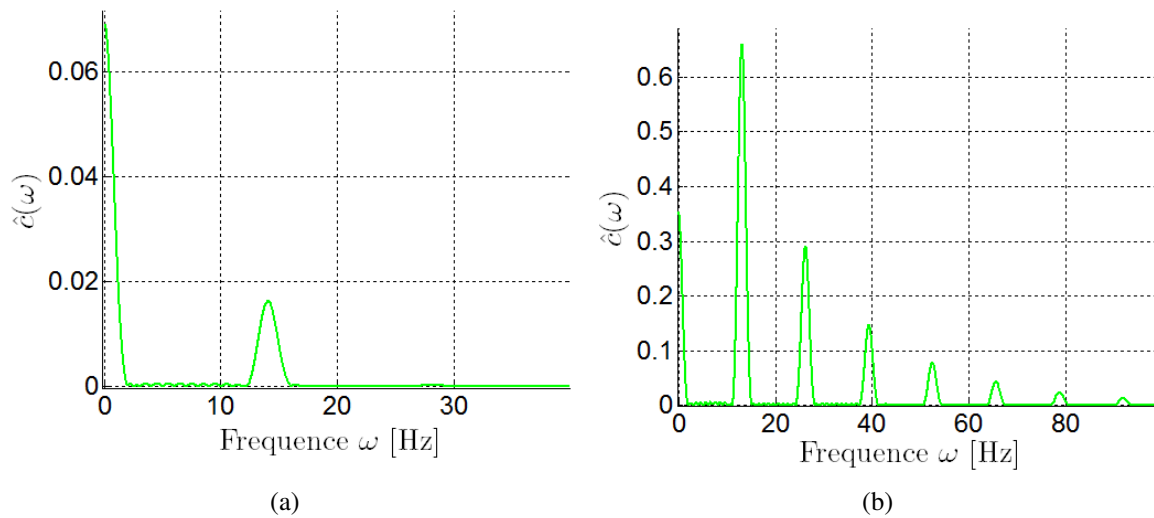


Figure 7: Motor-cart system: Fast Fourier Transform of the current over time (a) when $d = 0.001$ [m] and (b) when $d = 0.01$ [m].

found for the angular speed of the motor shaft, Fig. 6(a). It achieves a periodic state after a transient.

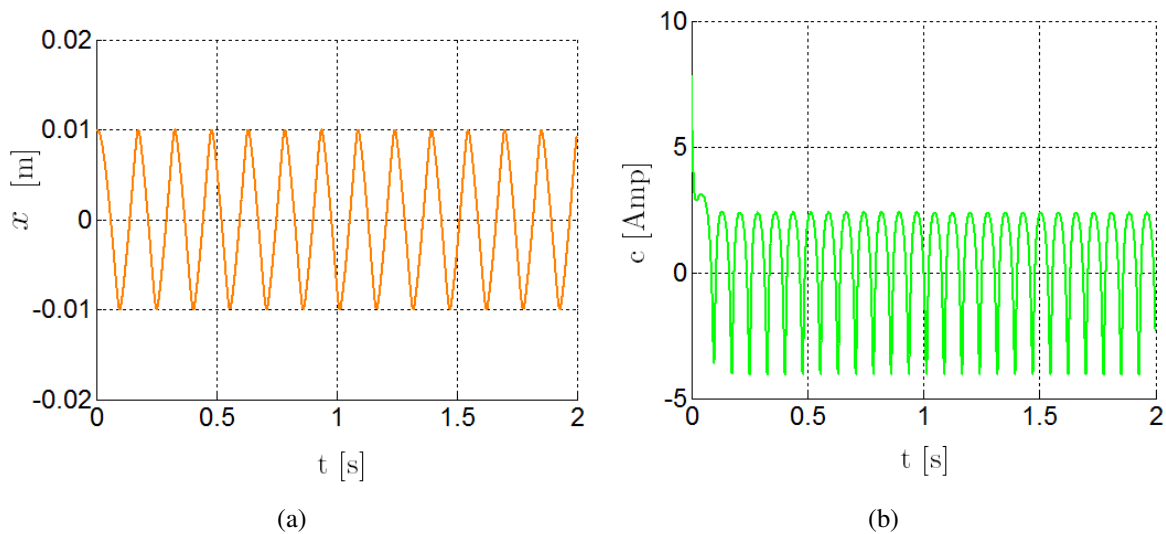


Figure 8: Motor-cart system with $d = 0.01$ [m]: (a) cart displacement and (b) motor current over time.

Others graphs to be analyzed are the $f(t)$ and $\tau(t)$ variation during one n -th cart movement cycle. This type of graph will be called *phase portrait*. The Fig. 9(a) and 9(b) shows these graphs for the fourth cycle, i.e., $n = 4$ and $\alpha(t) \in [8\pi, 10\pi]$.

Observing the f graph and remembering the constrain $x(t) = d \cos \alpha(t)$, it is verified that the horizontal force presents its maximum value when $x(t) = -d$ [m] and its minimum value when $x(t) = d$ [m]. Besides this, the cart positions corresponding to the points where f changes sign are $x(t) = -0.00415$ [m] and $x(t) = 0.00415$ [m]. At this values, the angular positions of the motor shaft, in the n -th cart movement cycle, are equals to $\alpha(t) = n2\pi + 1.99$ [rad] and $\alpha(t) = n2\pi + 5.14$ [rad].

Observing the τ graph, it is verified that the torque presents four points of sign changes. Two

of them occur when $x(t) = -d$ and $x(t) = d$, corresponding respectively to α multiple of π and α multiple of 2π . This changes were expected from Eq. (9). The others two changes occur exactly in the same cart positions that we have the f sign changing, i.e., when $x(t) = -0.00415$ [m] and $x(t) = 0.00415$ [m]. In each cart movement cycle, the horizontal force f and the torque τ follow once the paths shown in Fig. 9(a) and 9(b).

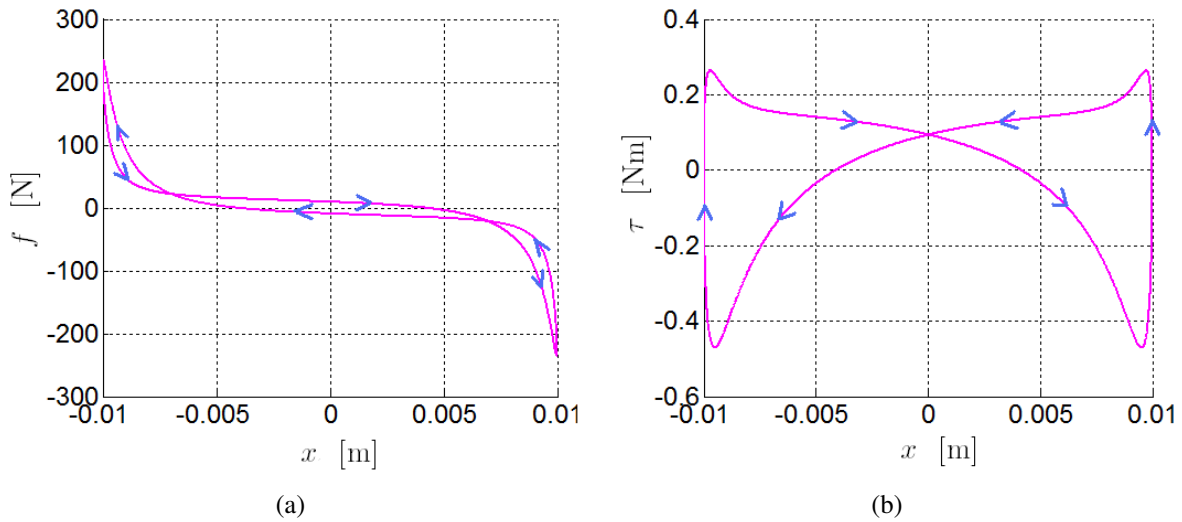


Figure 9: Motor-cart system with $d = 0.01$ [m]: (a) horizontal force f and (b) torque τ during one cycle of the cart movement.

The Fig. 10(a) and 10(b) show the graphs of the current variation during the fourth cart movement cycle and the torque variation in function of the current. In the left graph, it is noted that the current presents four points of sign changing. They occur when the x value are 0.00891 [m], -0.00728 [m], -0.00891 [m] and 0.00728 [m]. The corresponding angular positions of the motor shaft in the n -th cart movement cycle, α , at these points are $n2\pi + 0.47$ [rad], $n2\pi + 2.38$ [rad], $n2\pi + 3.61$ [rad] and $n2\pi + 5.53$ [rad].

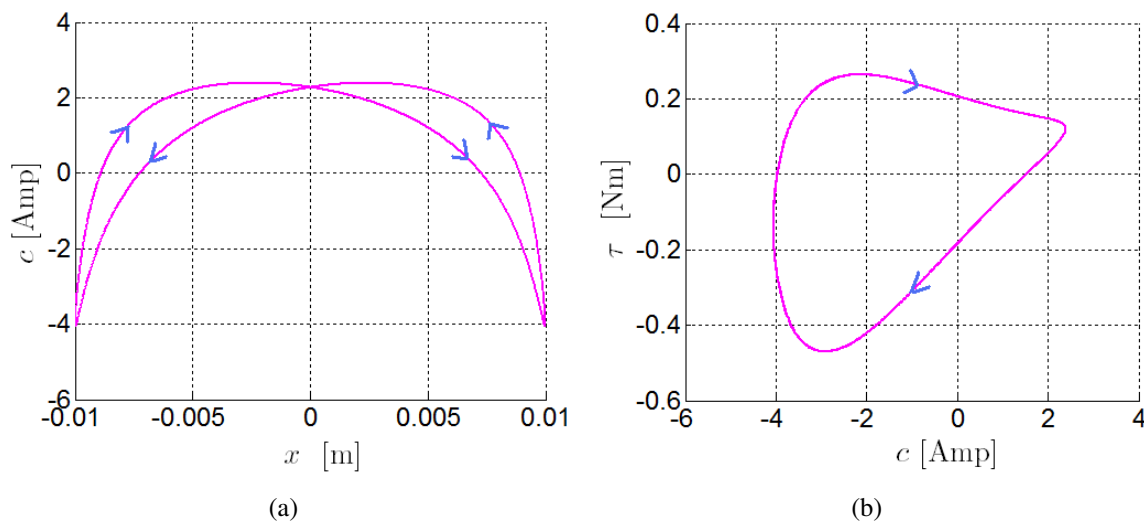


Figure 10: Motor-cart system with $d = 0.01$ [m]: (a) current variation during the fourth cart movement cycle and (b) torque variation in function of the current.

As the current presents four points of sign changing in each cart movement cycle, observing the graph of the torque variation in function of the current, it is verified that the current follows two times the path shown in Fig. 10(b). This result was expected since the FFT graph of \hat{c} presents a peak at a frequency that is twice the peak frequency of the FFT \hat{x} .

Others of the motor-cart system during the fourth cart movement cycle are shown in Fig. 11(a), 11(b), 12(a) and 12(b). The four points where the torque sign changes can be observed in the graph of torque in function of the coupling force. A similar behavior of Fig. 10(b) is found the graph of current in function of $\dot{\alpha}$. The current follows twice the path shown in Fig. 11(b).

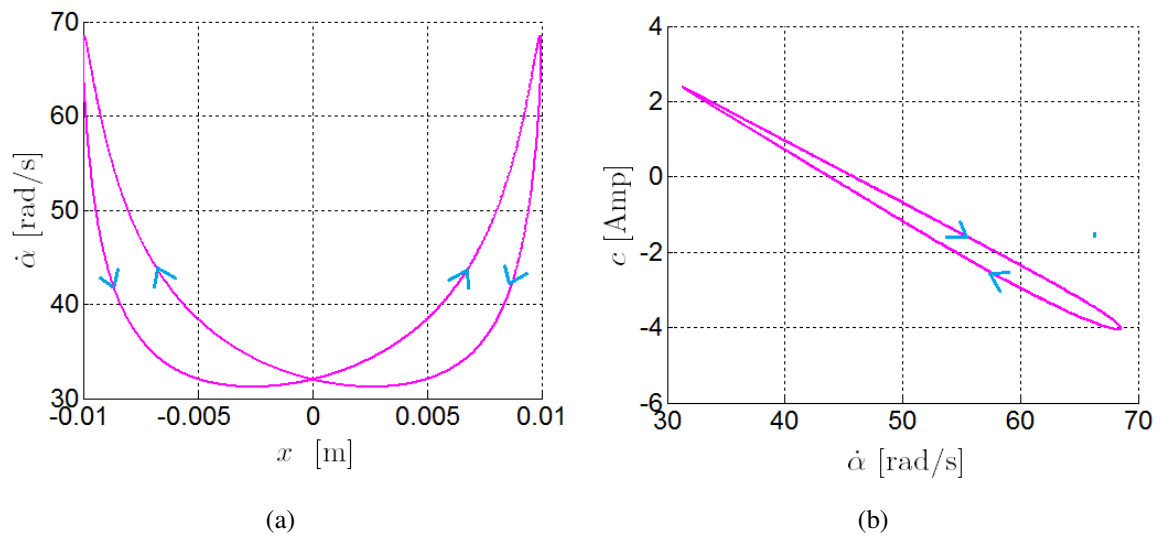


Figure 11: Motor-cart system with $d = 0.01$ [m]: (a) angular velocity of the motor shaft during the fourth cart movement cycle and (b) current variation in function of the angular velocity of the motor shaft.

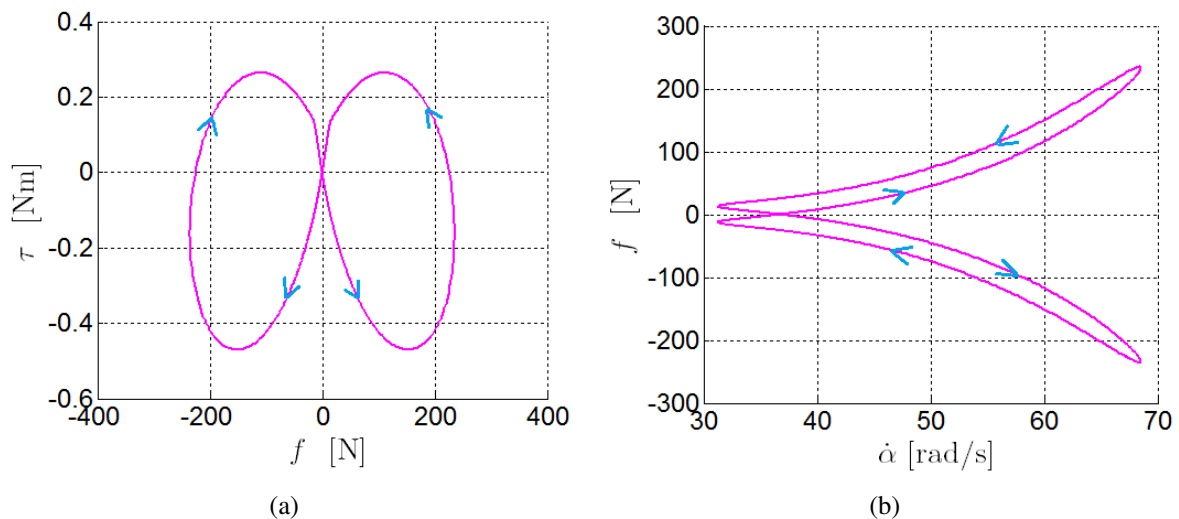


Figure 12: Motor-cart system $d = 0.01$ [m]: (a) torque variation in function of the horizontal force f and (b) horizontal force variation in function of the angular velocity of the motor shaft.

The angles where happen the sign changes of the horizontal force and current are represented in a circle graph in Fig. 13(a) and Fig. 13(b).

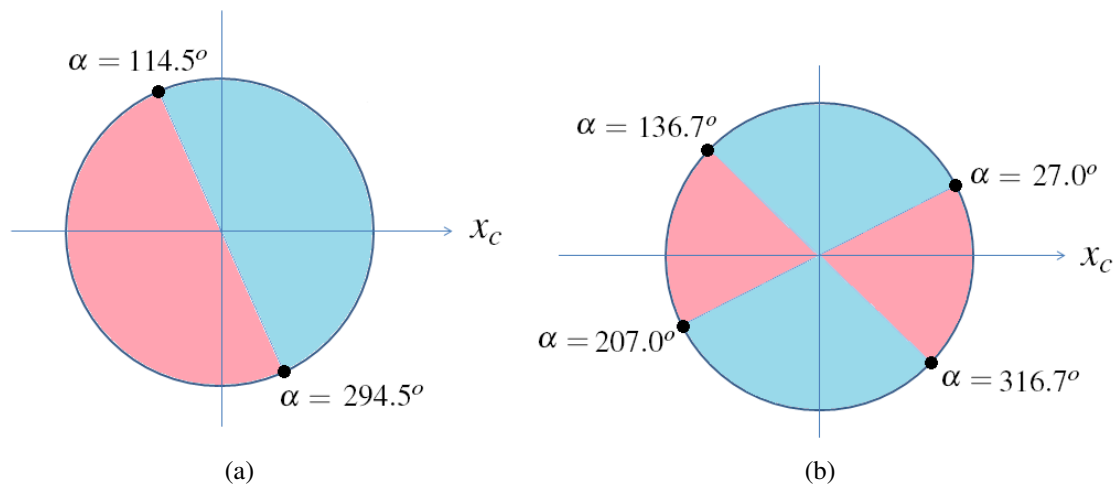


Figure 13: Motor-cart system $d = 0.01$ [m]: (a) angles α corresponding to the sign changes of the coupling horizontal force and (b) angles α corresponding to the sign changes of the current during one cart movement cycle. The blue parts correspond to the interval path where these variables are greater than zero, and the pink parts correspond to the interval path where they are smaller than zero.

3.2 Simulations of the motor-cart-pendulum system

A similar analysis to the one made to the motor-cart system was developed for the motor-cart-pendulum system.

Looking at the initial value problem Eq. (16), it is observed that if the nominal eccentricity of the pin, d , is small and the angle $\theta(t)$ is near zero, Eq. (16) tends to a linear system. But as the eccentricity grows, the nonlinearities become more pronounced. To better comprehend the increase of nonlinearities, the system Eq. (16), was integrated in a range of [0.0, 50.0] seconds for two different values of d : 0.001 [m] and 0.010 [m].

It was considered as initial conditions for the angular position and velocity of the motor shaft, $\alpha(0) = \dot{\alpha}(0) = 0.0$, and for the current in the motor $c(0) = v/r = 7.81$ [Amp] and for the angular position and velocity of the pendulum $\theta(0) = \dot{\theta}(0) = 0.0$. The specifications of the motor parameters used in the simulations are equal to the ones used in the simulations of the motor-cart system, listed in Table 1. The source voltage was assumed to be constant in time and equal to 2.4 [Volt]. The values of the cart and the pendulum masses were $m_c = 0.0$ [Kg] and $m_p = 5.0$ [Kg], so that the total mass, $m = m_c + m_p = 5.0$ [Kg], is equal to the embarked mass. Although the masses are equal, this configuration contrasts with the one of the motor-cart system used in the previous simulations. In spite of having the same masses, the pendulum has a relative motion with respect to the cart, and this make a huge difference. The pendulum length was assumed to be 0.075 [m].

The results obtained with the integration of Eq. (16), considering $d = 0.001$ [m], are shown in Fig. 14(a), 14(b), 15(a) and 15(b). These results reveal that when d is small, the angular speed of the motor shaft oscillates over time with a very small amplitude around 7 [Hz], the current also oscillates with a small amplitude around 0.13 [Amp], and the angular displacement of pendulum is near zero.

The Fast Fourier Transform was computed to the cart and pendulum displacements over time and to the current over time for this small value of d . It is noted that the FFT graph of \hat{x} , shown in Fig. 16(a), presents only one peak at the frequency at 7.04 [Hz]. This peak was expected, since this is close to the angular speed of the motor shaft. The FFT graph of $\hat{\theta}$ presents two peaks. One of them coincides with the \hat{x} peak and the other one is at the natural frequency of

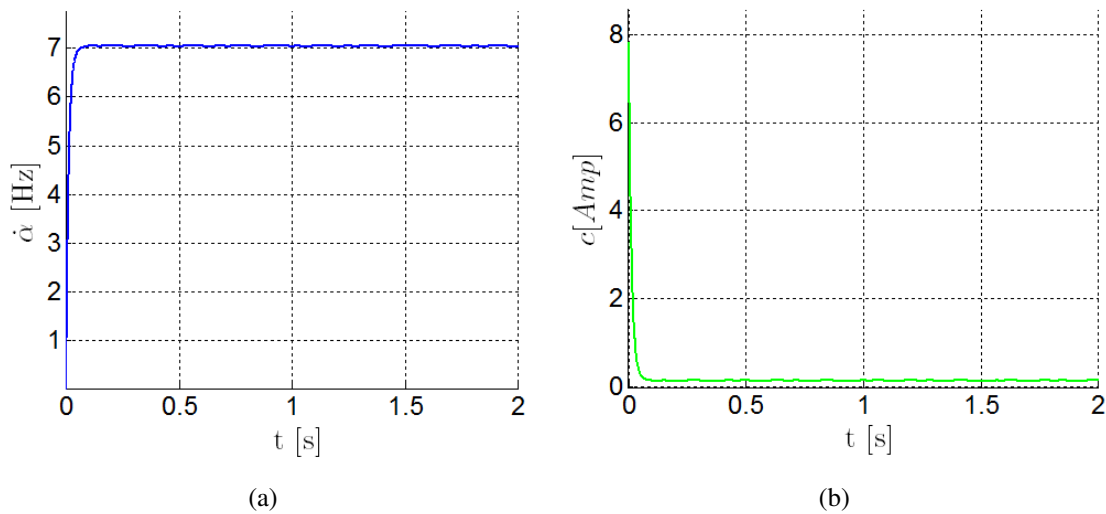


Figure 14: Motor-cart-pendulum system with $d = 0.001$ [m]: (a) angular velocity of the motor shaft and (b) current over time.

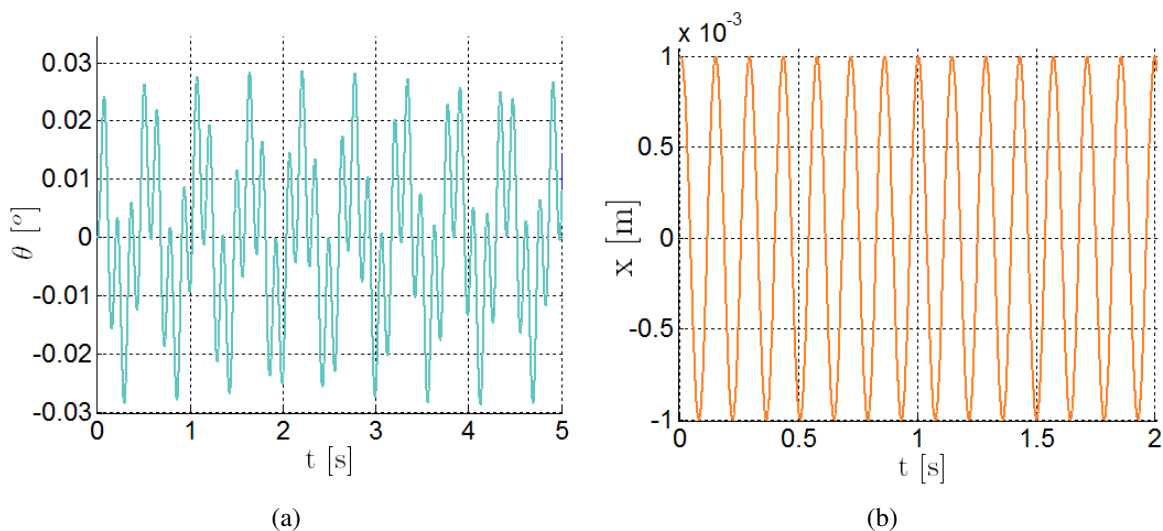


Figure 15: Motor-cart-pendulum system with $d = 0.001$ [m]: (a) pendulum and (b) cart displacement over time.

the pendulum, i.e., $\omega_n = \sqrt{g/l_p}/(2\pi) = 1.82$ [Hz]. The FFT graph of \hat{c} presents three peaks. One at 5.22 [Hz], one at 8.86 [Hz] and one at 14.08 [Hz], that is twice the peak frequency of the FFT \hat{x} . This relation between the peak frequency of \hat{c} and \hat{x} is equal to the relation found for the motor-cart-pendulum system.

When d is bigger, the amplitude of the oscillations of $\dot{\alpha}$, c , and θ are bigger when compared with the results obtained with the smaller d . Figures 17(a), 17(b), 18(a) and 18(b) show the angular speed of the motor, current, pendulum and cart displacement over time as result to the integration of Eq. 16 with $d = 0.01$ [m].

As done to the results with small d , the FFT was computed to the cart and pendulum displacements over time and to the current over time for the new value of d . It is noted that the graphs of \hat{x} and $\hat{\theta}$, shown in Fig. 19(a) and 19(b), present peaks at the same frequencies. The first of them is at 1.61 [Hz] and the following are at odd multiples of this value. Thus, comparing \hat{x} with $d = 0.001$ [m] and with $d = 0.01$ [m], it is verified that the peak at the natural

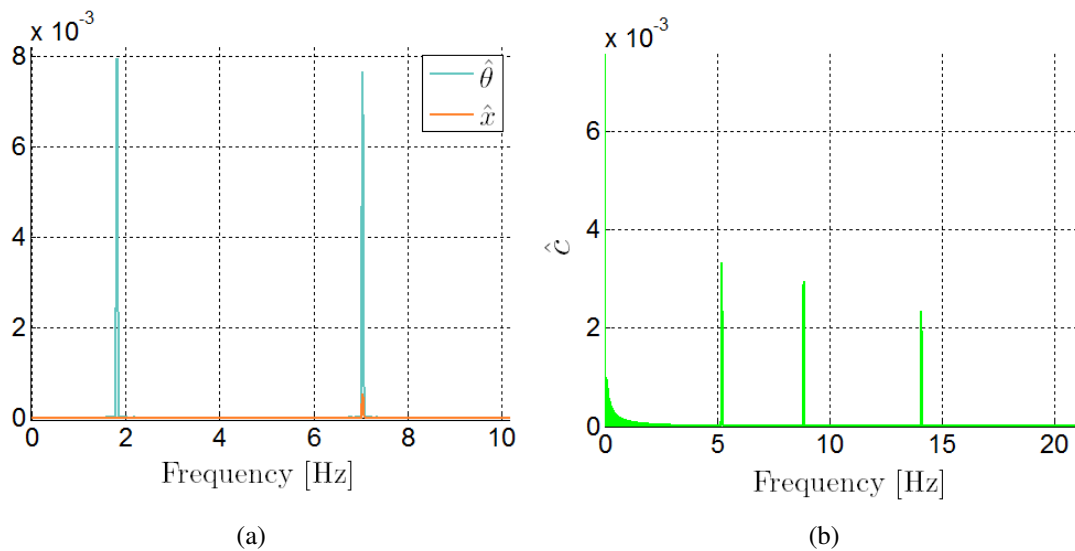


Figure 16: Motor-cart-pendulum system with $d = 0.001$ [m]: Fast Fourier Transform of (a) cart and pendulum displacements over time and (b) of current over time.

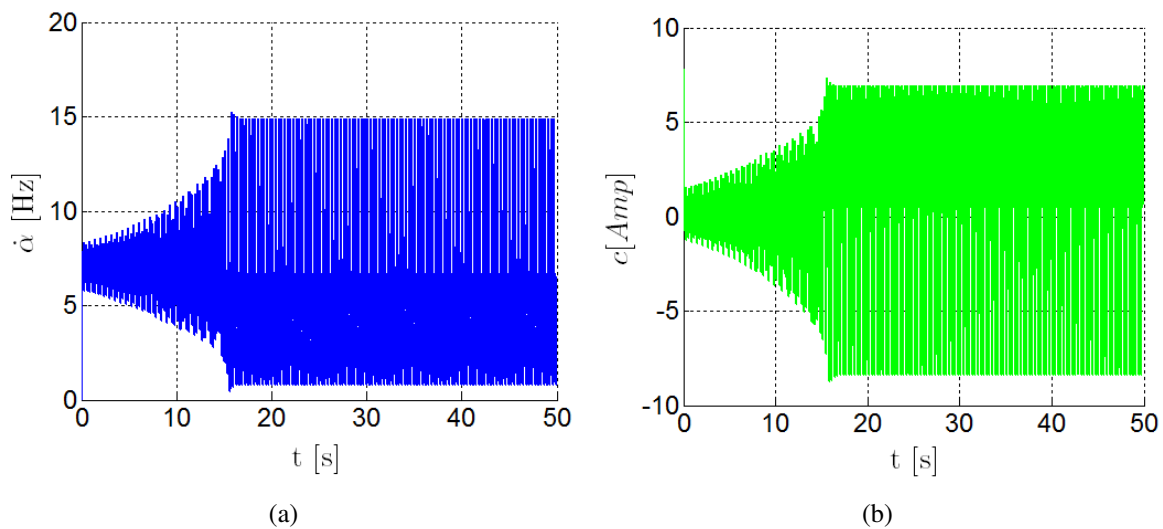


Figure 17: Motor-cart-pendulum system with $d = 0.01$ [m]: (a) angular velocity of the motor shaft and (b) current over time.

frequency of the pendulum, $\omega_n = 1.82$, vanished when d grows. This result certifies that the system behavior is far from linear.

The FFT graphs of the current and of the angular speed of the motor shaft over time also present peaks at the same frequencies. The first of them is at 3.21 [Hz] and the following are at multiples of this value, as shown in Fig. 20(a) and 20(b). Comparing this first peak frequency, 3.21 [Hz], with the first peak frequency found for $\hat{\theta}$ and \hat{x} , 1.61 [Hz], it is verified that the same phenomenon found for the motor-cart system is found for the motor-cart-pendulum system. The \hat{c} presents a first peak at a frequency that is twice the peak frequency of the FFT for \hat{x} .

This non-periodic behavior presents reflects in the graphs of f , τ and c during one cart movement cycle and in the graph of torque variation in function of the current. Figures 21(a), 21(b), 22(a) and 22(b) show these four graphs for the last cycle in the period [0, 50] seconds of the integration of Eq. 16.

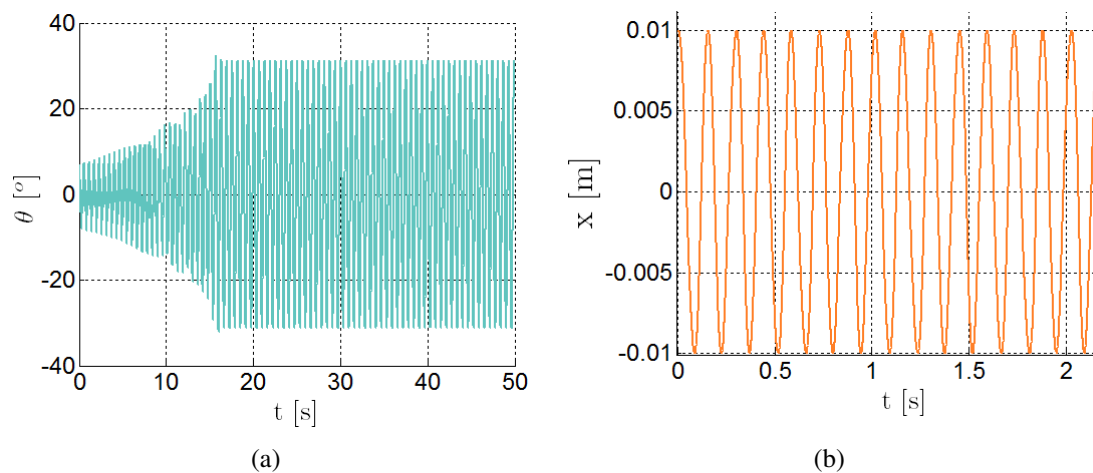


Figure 18: Motor-cart-pendulum system with $d = 0.01$ [m]: (a) pendulum and (b) cart displacement over time.

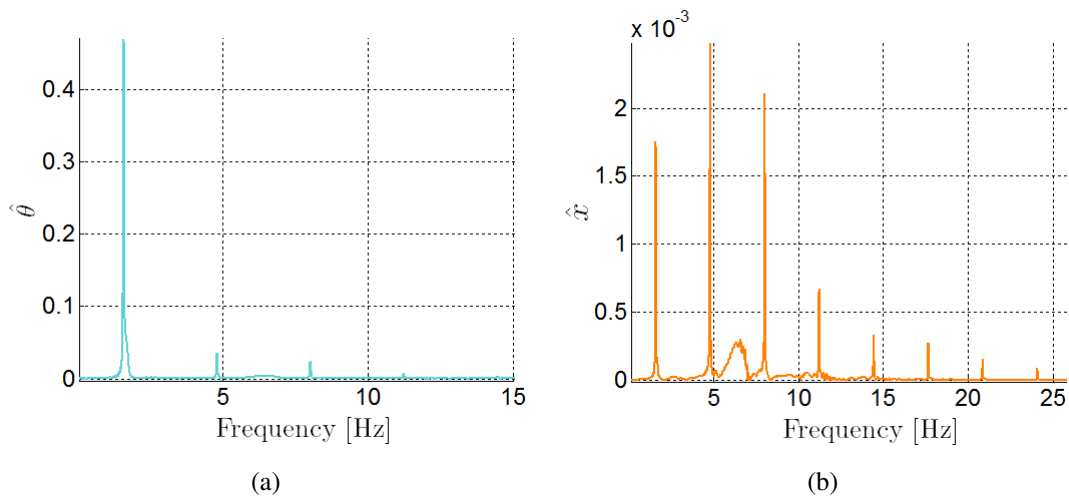


Figure 19: Motor-cart-pendulum system with $d = 0.01$ [m]: Fast Fourier Transform of (a) pendulum and (b) cart displacements over time.

It is possible to observe that the graphs of τ and c have lost their symmetry in relation to a vertical axis drawn at $x = 0$ and the graph of torque variation in function of the current is no longer a closed path. Similar effects are noted in the phase portraits in the last cart movement cycle of $\dot{\alpha}$ in function of x , c in function of $\dot{\alpha}$, τ in function of f and f in function of $\dot{\alpha}$. These graphs are shown in Fig. 23(a), 23(b), 24(a) and 24(b).

The graphs of the coupling force, f , and coupling torque, τ , over time are presented in Fig. 25(a) and 25(b).

4 PUMPING LEADS TO REVOLUTION

In the analysis developed to the the motor-cart-pendulum system, in the previous section of the paper, the cart mass was considered to be zero and the pendulum mass 5.0[Kg]. Next, it is presented an analysis of the behavior of this system with a different mass configuration. The cart mass is kept as 0.0 [Kg] and a smaller value is selected to the pendulum mass, $m_p = 4.0$ [Kg], so that the total mass, $m_c + m_p = 4.0$ [Kg], is still equal to the embarked mass.

To observe the influence of this new configuration in the system behavior, the Eq. 16 was

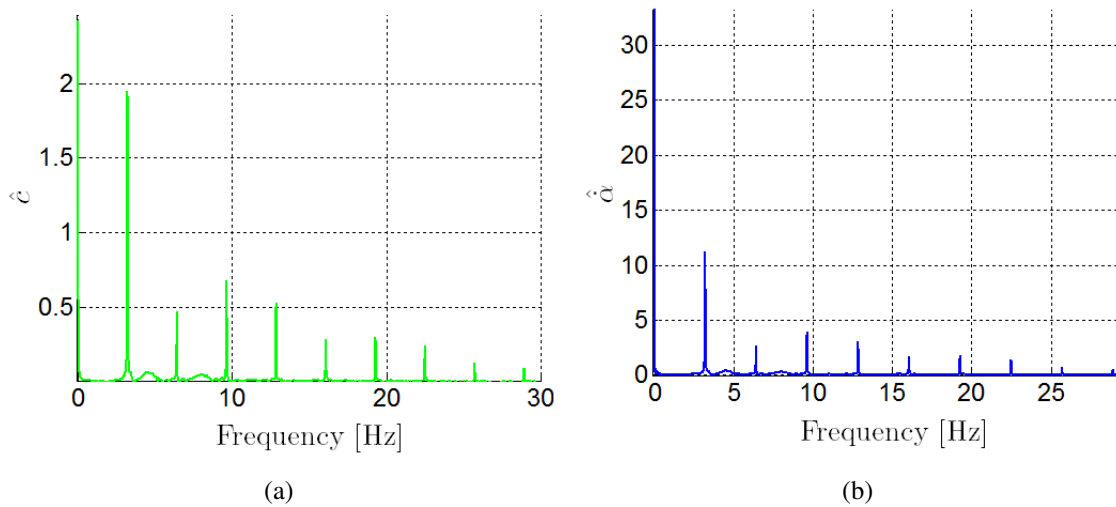


Figure 20: Motor-cart-pendulum system with $d = 0.01$ [m]: Fast Fourier Transform of (a) current and (b) angular speed of the motor shaft over time.

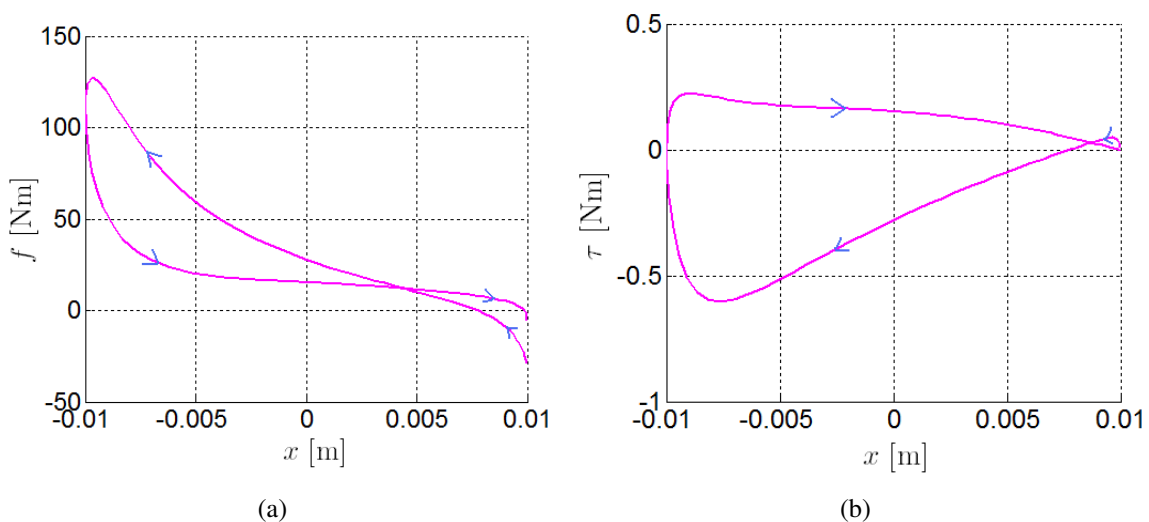


Figure 21: Motor-cart-pendulum system with $d = 0.01$ [m]: (a) horizontal force f and (b) torque τ during the last cycle of the cart movement.

integrated in a range of $[0, 50]$ seconds with the null initial conditions to $\alpha(0)$, $\dot{\alpha}(0)$, $\theta(0)$ and $\dot{\theta}(0)$. The initial current was considered equal to $c(0) = v/r = 7.81$ [Amp] and the nominal pin eccentricity 0.01 [m]. The source voltage was assumed to be constant in time and the specifications of the motor parameters are listed in Table 1.

The obtained results for the angular speed of the motor shaft, for the current and cart and pendulum displacements are shown in Fig. 26(a), Fig. 26(b), Fig. 27(a) and Fig. 27(b). The mechanical system pumps energy from the motor and the amplitude of the pendulum grows reaching a point where the mechanical system starts to drive the motion, Gourdon et al. (2007); Gourdon (2006); Cataldo et al. (2012). This is seen nothing that $\dot{\alpha}$ takes negatives values, meaning that the motor shaft changes its motion direction sometimes. When the angular speed of the motor shaft is positive, it is considered that the motor drives the cart motion, the cart is driven. But in the period when it is negative, the motor loses the control over the cart and drives it no more, it is now driven by the mechanical system. In these situations, it will be said

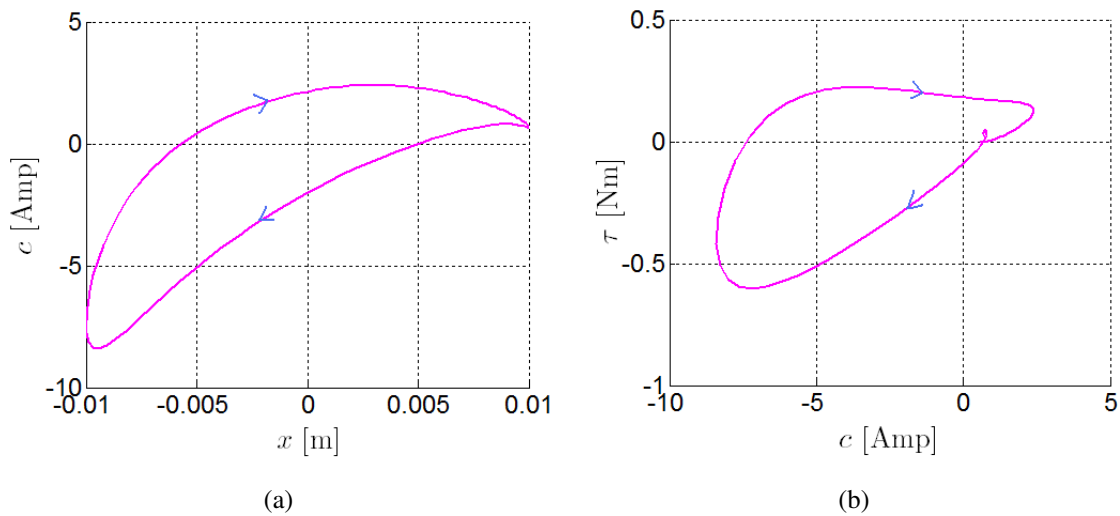


Figure 22: Motor-cart-pendulum system with $d = 0.01$: (a) current variation during the last cart movement cycle and (b) torque variation in function of the current.

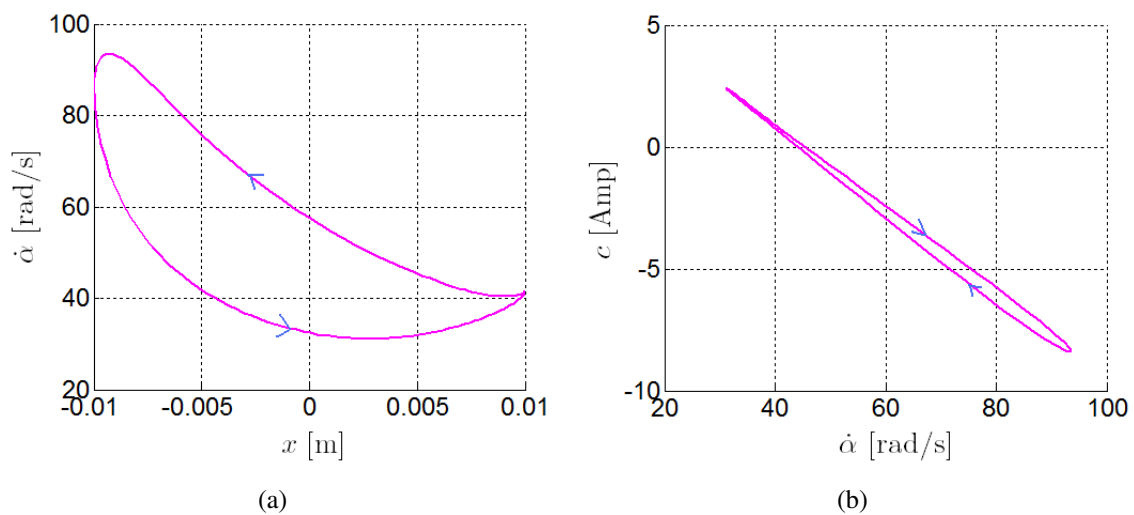


Figure 23: Motor-cart-pendulum system with $d = 0.01$ [m]: (a) angular velocity of the motor shaft during the last cart movement cycle and (b) current variation in function of the angular velocity of the motor shaft.

that the relation master-slave is reverted.

To better comprehend the sign changing of the angular speed of the motor shaft, some phase portrait graphs were plotted. Figures 28(a) and 28(b) show the $\ddot{\alpha}$ graph in function of $\dot{\alpha}$ and the $\dot{\alpha}$ graph in function of x during one movement cycle. It is verified that when $\dot{\alpha}(t)$ turns negative, the motor shaft has a negative acceleration. After a short period of time, its acceleration becomes positive and brakes the motor shaft motion. This causes other sign changing in $\dot{\alpha}(t)$ and consequently, it turns positive again. Thus, the motor recovers the control over the cart motion.

Looking at Fig. 28(b), it is noted that this reversion in the relation master-slave occurs two times in each movement cycle. The position and angular speed of the pendulum, at the moment of the reversion, can be discovered by the graphs of $\dot{\theta}$ in function of $\dot{\alpha}$ and θ in function of $\dot{\alpha}$. They are shown in Fig. 29(a) and 29(b). It is verified that when the the motor loses the control over the cart by the sign changing of $\dot{\alpha}$, the pendulum angle is around 21.6 [°] or around -21.6

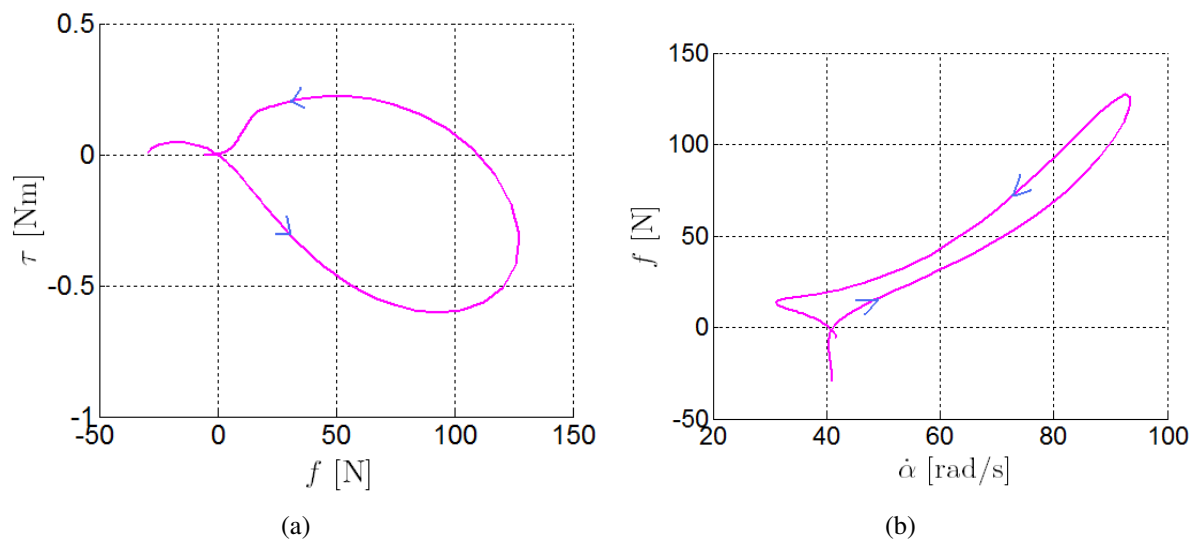


Figure 24: Motor-cart-pendulum system with $d = 0.01$ [m]: (a) torque variation in function of the coupling force and (b) f variation in function of the angular velocity of the motor shaft.

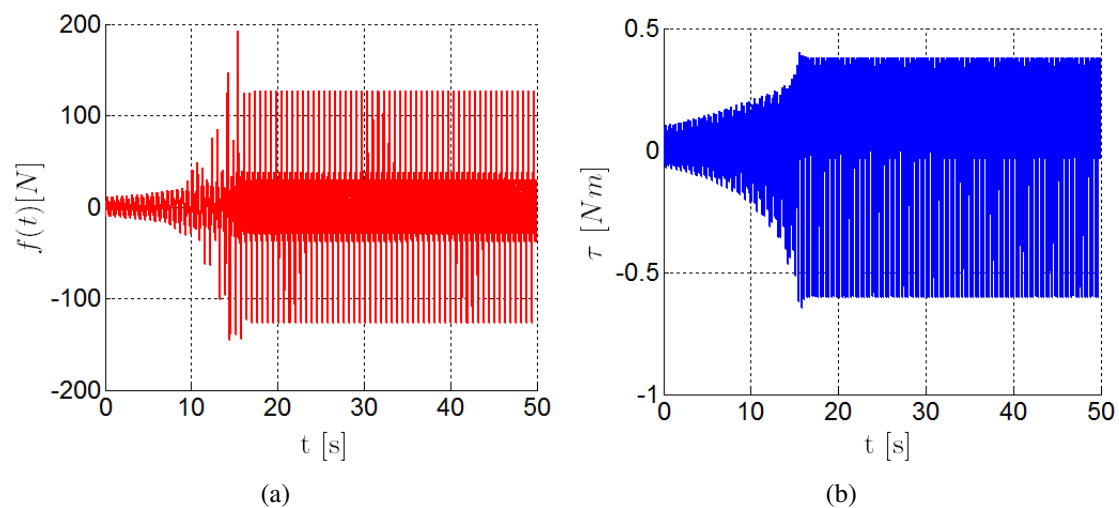


Figure 25: Motor-cart-pendulum system with $d = 0.01$ [m]: (a) coupling force, f , and (b) torque over time, τ .

[$^{\circ}$]. When the motor recovers the control, the pendulum angle is around 6.0 [$^{\circ}$] or around -6.0 [$^{\circ}$].

It is also noted that, during the period of reversion, the pendulum does not change its direction of motion in spite of its angular speed presents a change of behavior. In the beginning of the reversion the modulus of $\dot{\theta}$ grows, but when it achieves the value 2.95 [Hz], it starts to decrease. This change occurs due to the sign changing in the tangent angular acceleration of the pendulum, as can be observed in Fig. 30(a). The graph of the torque variation in function of the angular speed of the motor shaft shows that the maximum torque is achieved during the period of reversion.

5 PROBABILISTIC MODEL

To make a stochastic analysis of the two proposed systems, a system parameter is considered uncertain. It is assumed that the value of the nominal eccentricity of the pin, d is a random

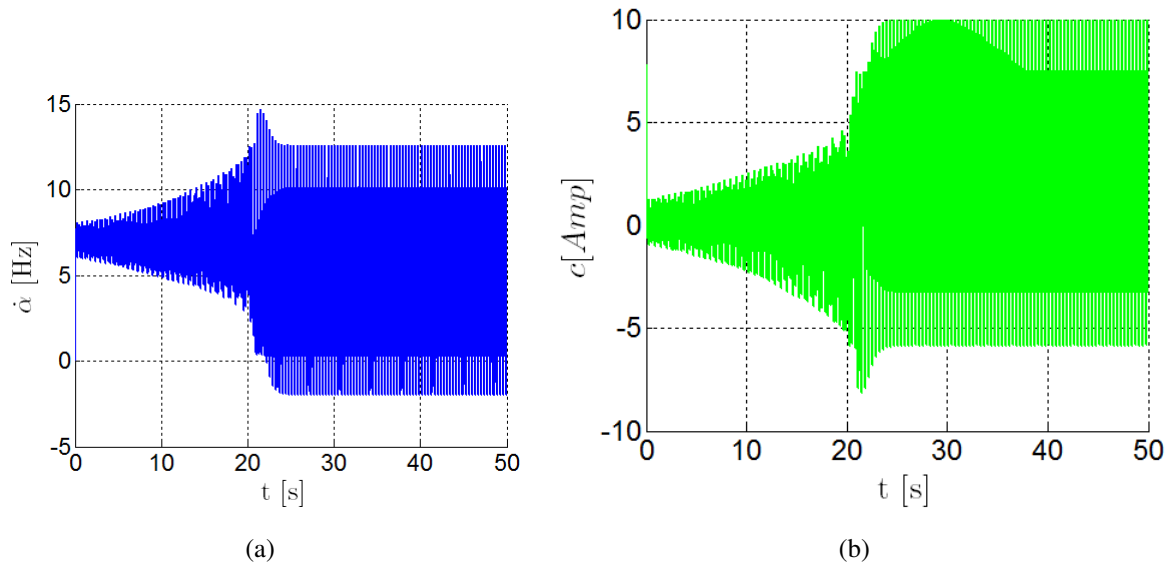


Figure 26: Motor-cart-pendulum system with $d = 0.01$ [m]: (a) angular velocity of the motor shaft and (b) current over time.

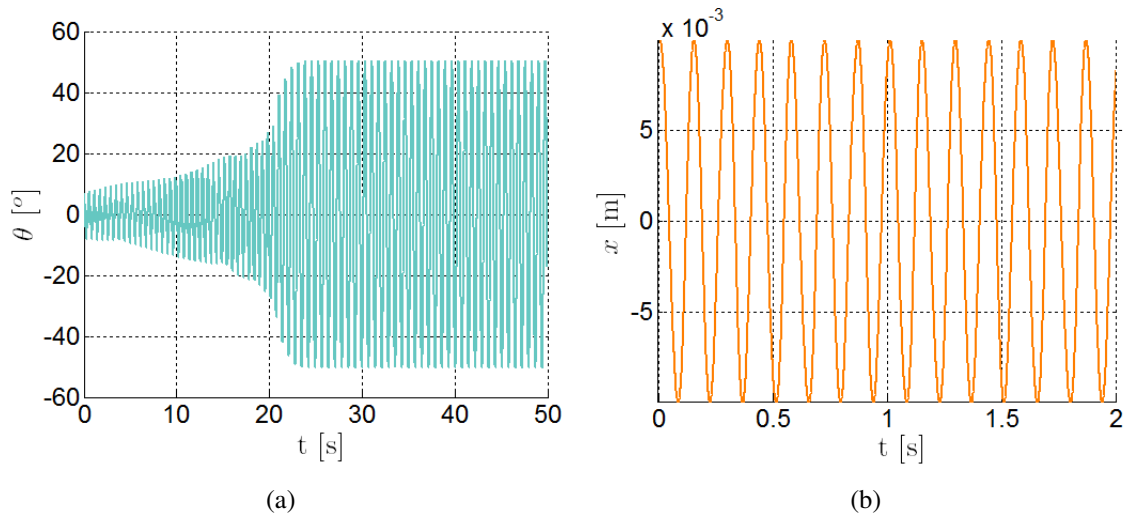


Figure 27: Motor-cart-pendulum system with $d = 0.01$ [m]: (a) pendulum and (b) cart displacement over time.

variable represented by the capital letter D .

The Maximum Entropy Principle (PEM) is used to construct the probability density function of this random variable (Jaynes, 1957; Shannon, 1948; Sampaio and de Queiroz Lima, 2012; de Cursi and Sampaio, 2012) and it is assumed that the only available information is the support of D : $[d_{min}, d_{max}]$. Therefore, the Maximum Entropy Principle using Shannon entropy measure of the probability density function, p , of D , $S(p) = - \int_{d_{min}}^{d_{max}} \ln(p(d))p(d) dp$, yields the uniform probability density function, given by

$$p(d) = \mathbb{1}_{[d_{min}, d_{max}]}(d) \frac{1}{d_{max} - d_{min}}. \quad (18)$$

where $\mathbb{1}_{[d_{min}, d_{max}]}(d)$ is an indicator function that is equal to 1 for $d \in [d_{min}, d_{max}]$ and 0 otherwise.

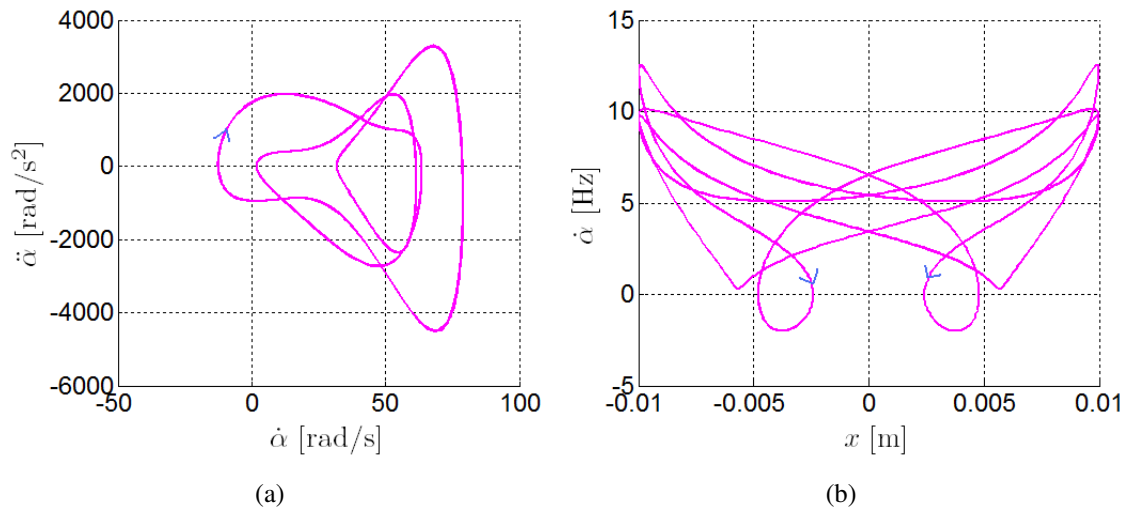


Figure 28: Motor-cart-pendulum system with $d = 0.01$ [m]: portrait graphs of (a) $\ddot{\alpha}$ graph in function of $\dot{\alpha}$ and (b) $\dot{\alpha}$ graph in function of x .

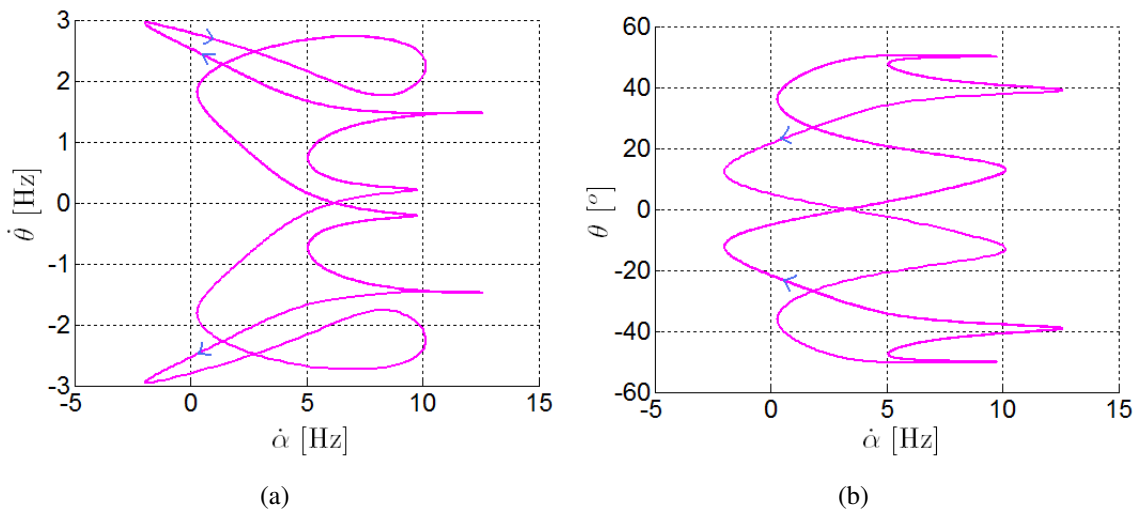


Figure 29: Motor-cart-pendulum system with $d = 0.01$ [m]: portrait graphs of (a) $\dot{\theta}$ graph in function of $\dot{\alpha}$ and (b) θ in function of $\dot{\alpha}$.

6 NUMERICAL SIMULATIONS OF THE STOCHASTIC SYSTEMS

As it was assumed that the value of the nominal eccentricity of the pin is a random variable, the output variables of the stochastic coupled systems are random process with parameter t . Therefore, the horizontal cart displacement is represented by the random process \mathcal{X} , the pendulum displacement by Θ , the angular displacement of the motor shaft by \mathcal{A} , the angular velocity of the motor shaft by $\dot{\mathcal{A}}$, the current by \mathcal{C} , the horizontal force by \mathcal{F} and the torque by \mathcal{T} .

To make the stochastic analysis of the two coupled systems, Monte Carlo simulations were employed to compute the mean and variance of the the random processes listed above. The support of D was assumed to be $[d_{min}, d_{max}] = [0.005, 0.015]$ (units in [m]).

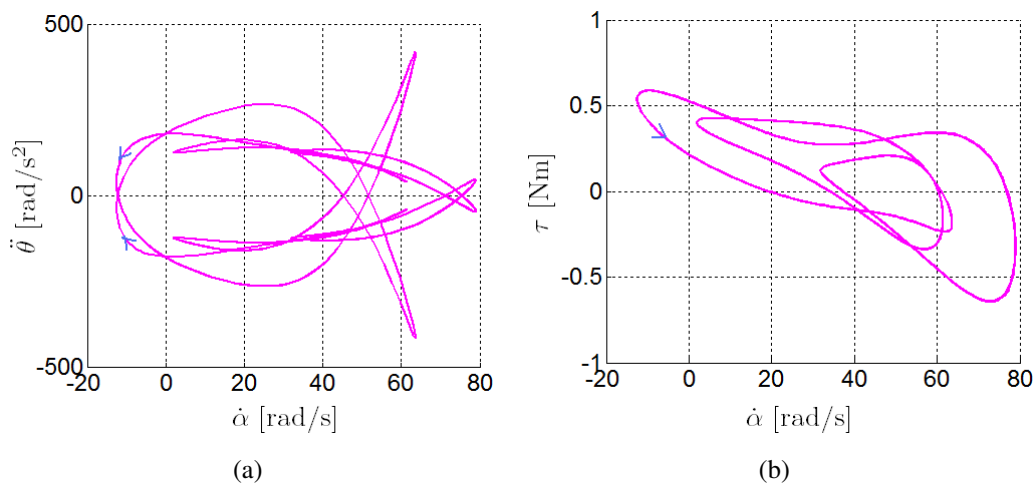


Figure 30: Motor-cart-pendulum system with $d = 0.01$ [m]: portrait graphs of (a) tangent $\ddot{\theta}$ graph in function of $\dot{\alpha}$ and (b) τ in function of $\dot{\alpha}$.

6.1 Stochastic simulations of the motor-cart system

Figures 31(a), 31(b), 32(a) and 32(b) show the envelope graphs of \mathcal{C} , $\dot{\mathcal{A}}$, \mathcal{X} and \mathcal{F} constructed with 2×10^3 realizations of these random process. In each realization, the system Eq. (11), was integrated in a range of [0.0, 3.0] seconds. The cart mass was considered to be $m_c = 5.0$ [Kg], the source voltage 2.4 [Volt] and, the specifications to the motor parameters are listed in Table 1.

It is possible observe that the variations on the value of the nominal eccentricity of the pin bring significant dispersions to the oscillation amplitudes and to the oscillation frequencies of the output variables.

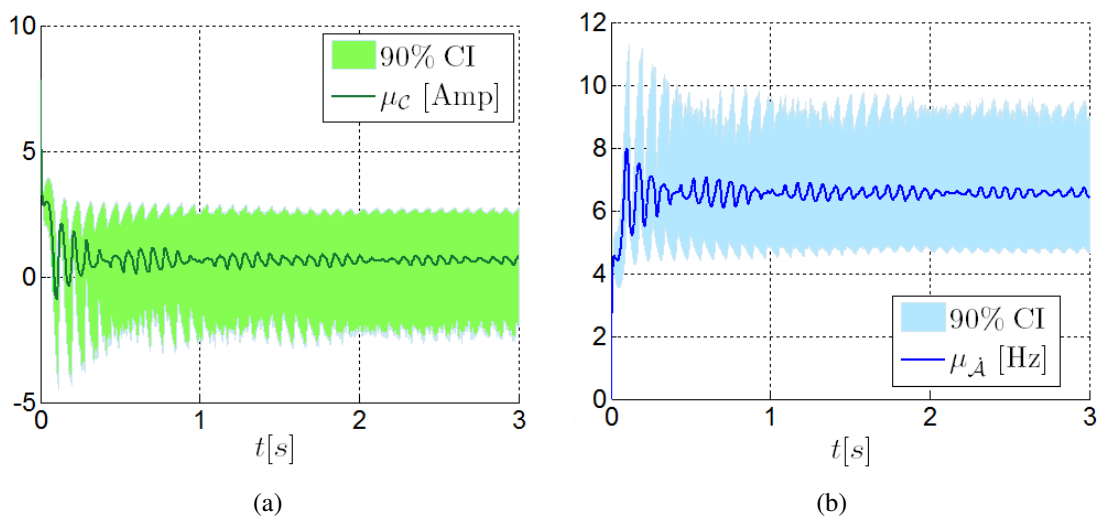


Figure 31: Motor-cart system: (a) Envelope graphs of \mathcal{X} and $\dot{\mathcal{A}}$.

6.2 Stochastic simulations of the motor-cart-pendulum system

Figures 33(a), 33(b), 34(a) and 34(b) show the envelope graphs of \mathcal{C} , $\dot{\mathcal{A}}$, \mathcal{X} and Θ constructed with 2×10^3 realizations of these random process. In each realization, the system

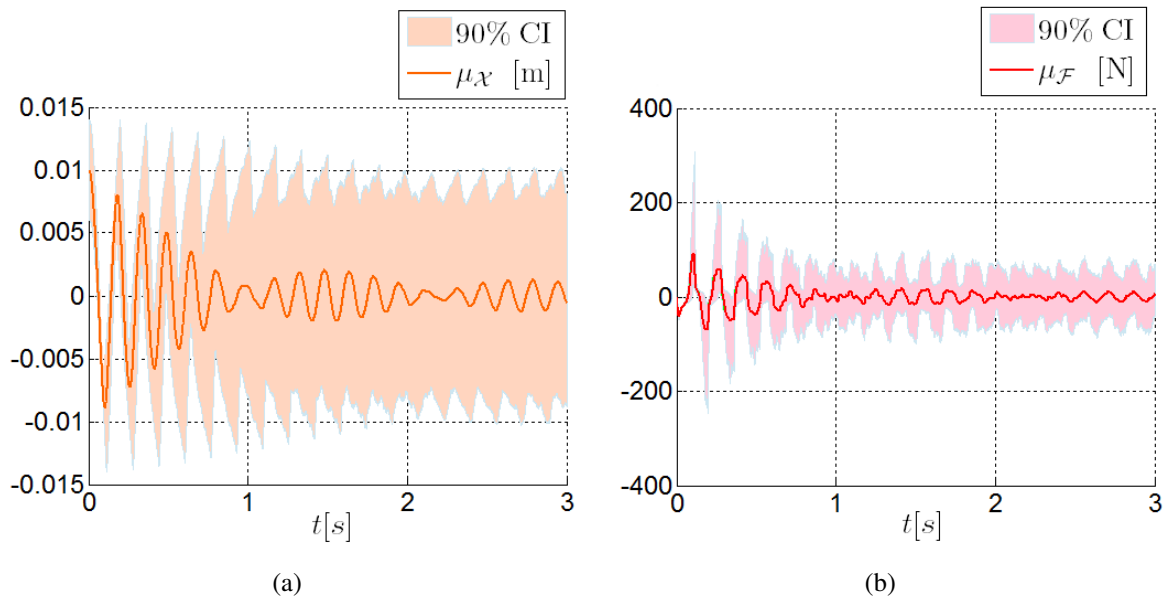


Figure 32: Motor-cart system: (a) Envelope graphs of \mathcal{X} and \mathcal{F} .

Eq. (16), was integrated in a range of [0.0, 1.0] seconds. The cart mass was considered to be $m_c = 1.0$ [Kg], the pendulum mass $m_p = 4.0$ [Kg], the pendulum length $l_p = 0.075$ [m], the source voltage 2.4 [Volt] and, the specifications to the motor parameters are listed in Table 1.

It is possible observe that the variations on the value of the nominal eccentricity of the pin bring significant dispersions to the oscillation amplitudes of the output variables. The dispersions relative to the oscillation frequencies are small, meaning that the variations on d do not have an big impact on this parameter in the period of [0.0, 1.0] seconds. If the period of integration of Eq. (16) were bigger, probably, the impact of the variations on d would be huge. As shown in the deterministic analysis of the motor-cart-pendulum system, the FFT graphs of \hat{x} , $\hat{\theta}$ and \hat{c} are very sensitive to variation of the parameter d .

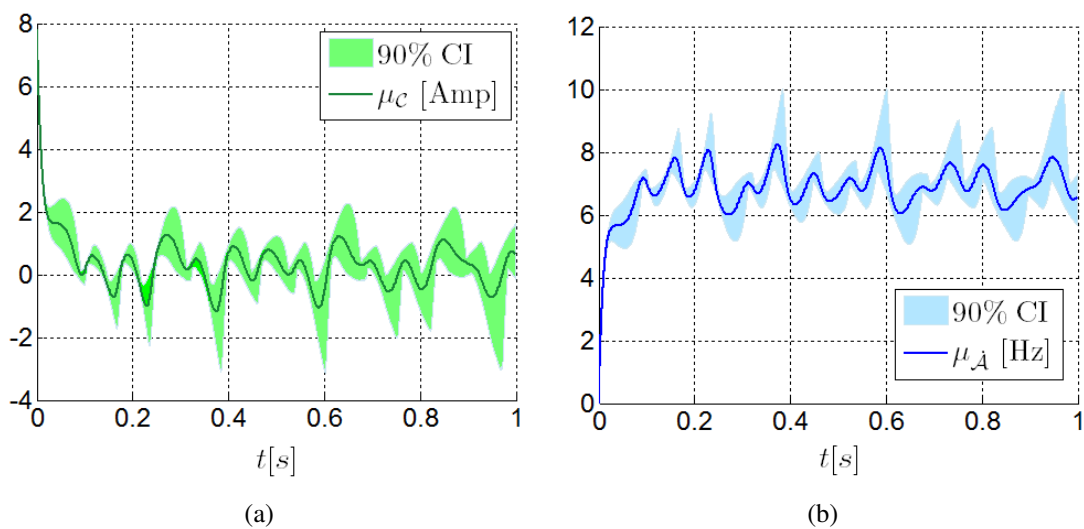


Figure 33: Motor-cart-pendulum system: (a) Envelope graphs of \mathcal{C} and $\dot{\mathcal{A}}$.

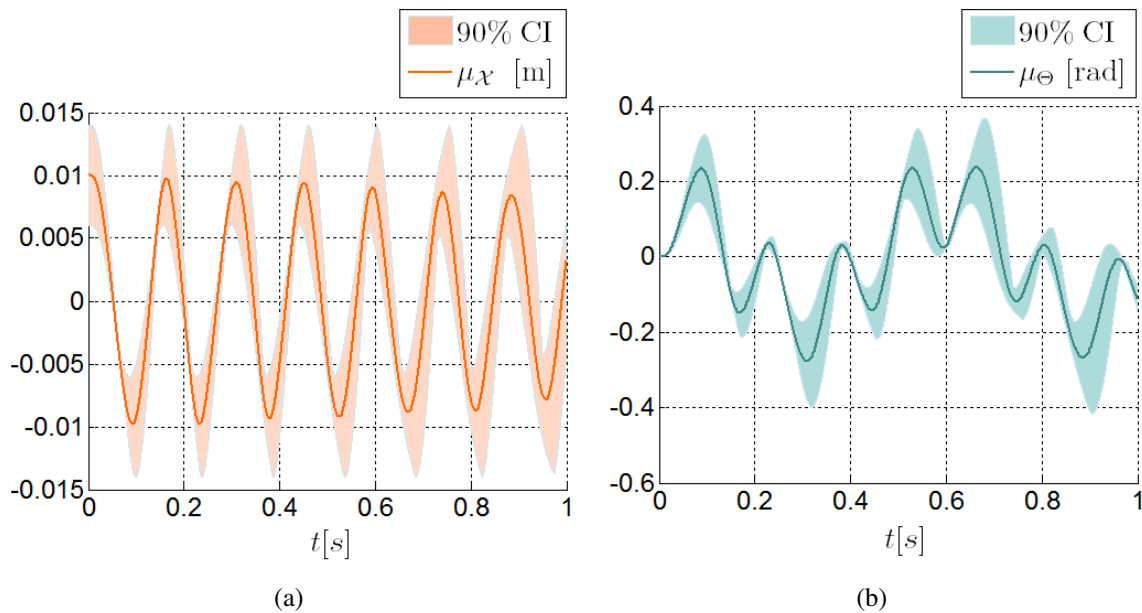


Figure 34: Motor-cart-pendulum system: (a) Envelope graphs of \mathcal{X} and Θ .

7 CONCLUSIONS

The purpose of this paper was to analyze and compare the behavior of two electromechanical systems. The first one is composed by a cart whose motion is driven by a DC motor and in the second one a embarked mass, a pendulum, was into the cart. The motor-cart system has no capacity to pump energy from the motor, it is a master-slave system: the motor drives the cart motion, the cart is driven. The only interesting feature is how the nonlinearity changes with d and m , the mass of the cart. The nonlinearity of the coupled system comes from the coupling. The motor-cart-pendulum system has a new feature, the capacity to store energy in the motion of the pendulum. With this the mechanical system can pump energy from the motor and, in certain cases, revert the relation master-slave, that is the mechanical system can be itself the master stopping the motor and reverting its motion. For the motor-cart-pendulum system, for a fixed mass $m = m_c + m_p$, the relation between m_c and m_p is important. The study of the relation and how it affects the dynamics will be object of a future work. The influence of a embarked mass was demonstrated and it was shown the changes it causes in the solutions of the dynamic equations.

The nominal eccentricity of the pin of the motor, d , was characterized as a parameter that controls the nonlinearities of the equations of motion of both systems, and its influence in the dynamic equations was analyzed by the Fast Fourier Transform.

In the stochastic analysis, d was modeled as a random variable and the Maximum Entropy Principle was used to construct the probability model. Monte Carlo simulations were employed to compute the mean and the 90% confidence interval of the displacements of the random process that characterize the output variables of the stochastic coupled systems. It was observed that the most important effect of the variations on d were the generation of dispersions to the oscillation amplitudes and frequencies of the output variables.

As future work, a study of the distribution of mass between the cart and the pendulum in the motor-cart-pendulum system will be done. In this paper, the total mass of the motor-cart-pendulum system was considered equal to the embarked mass, a extreme case. So would be

interesting to study others configurations. Another work in preparation is to investigate the influence of dissipation in the mechanical system, specially of the friction between the pin and the slot machined on the acrylic plate in the coupling mechanism.

8 ACKNOWLEDGMENTS

This work was supported by the Brazilian Agencies CNPQ, CAPES and FAPERJ.

REFERENCES

- Aguiar R. *Experimental investigation and numerical analysis of the vibro-impact phenomenon*. Ph.D. thesis, PUC-Rio, Rio de Janeiro, Brazil, 2010.
- Balthazar J., Mook D., Weber H., Brasil R., Felini A., Belato D., and Felix J. An overview on non-ideal vibrations. *Meccanica*, 38:613–621, 2003.
- Belato D. *Análise Não Linear de Sistemas Dinâmicos Holônomo Não Ideais*. PhD thesis, Department of Mechanical Engineering, Universidade Estadual de Campinas, Campinas, S.P., Brazil, 2002.
- Cataldo E., Bellizzi S., and Sampaio R. Free vibrations of an uncertain energy pumping system. Technical report, PUC-Rio, 2012.
- de Cursi E.S. and Sampaio R. *Modelagem Estocástica e Propagação de Incertezas*. Notas de Matemática Aplicada. SBMAC, 2012.
- Evan-Iwanowski R.M. *Resonance oscillations in mechanical systems*. Elsevier Publ. Co., Amsterdam, 1976.
- Fidlin A. *Nonlinear Oscillations in Mechanical Engineering*. Springer, Netherlands, 2006.
- Gourdon E. *Contrôle passif de vibrations par pompage énergétique*. Ph.D. thesis, Ecole Centrale de Lyon, 2006.
- Gourdon E., Alexander N., Taylor C., Lamarque C., and Pernot S. Nonlinear energy pumping under transient forcing with strongly nonlinear coupling: Theoretical and experimental results. *Journal of Sound and Vibration*, 300:522–551, 2007.
- Hagedorn P. *Non-linear Oscillations*. Clarendon Press, Oxford, second edition, 1988.
- Jaynes E. Information theory and statistical mechanics. *The Physical Review*, 106(4):620–630, 1957.
- Karnopp D., Margolis D., and Rosenberg R. *System Dynamics: Modeling and Simulation of Mechatronic Systems*. John Wiley and Sons, 4th edition, New-York, USA, 2006.
- Kononenko V.O. *Vibrating Systems with a Limited Power Supply*. London Iliffe Books LTD, England, 1969.
- Lacarbonara W. and Antman S. What is parametric excitation in structural dynamics? In *ENOC-2008*. ENOC, Saint Petersburg, Russia, 2008.
- Nayfeh A.H. and Mook D.T. *Nonlinear Oscillations*. John Wiley and Sons, USA, 1979.
- Rocard Y. *Dynamique Générale des Vibrations*. Masson et Cie., Éditeurs, Paris, France, 1943.
- Sampaio R. and de Queiroz Lima R. *Modelagem Estocástica e Geração de Amostras de Variáveis e Vetores Aleatórios*. Notas de Matemática Aplicada. SBMAC, 2012.
- Shannon C. A mathematical theory of communication. *Bell System Tech.*, 27:379–423 and 623–659, 1948.
- Troger H. and Steindl A. *Nonlinear Stability and Bifurcation Theory: An Introduction for Engineers and Applied Scientists*. Springer-Verlag, Wien, 1991.